Research in Astron. Astrophys. **2013** Vol. **13** No. **7**, 841–848
http://www.raa-journal.org *http://www.iop.org/journals/raa*

Research in Astronomy and Astrophysics

Radiative transfer modeling of three T Tauri stars: selecting candidates for studying circumstellar disk evolution *

Yao Liu[1,2,3], Hong-Chi Wang[1], Sebastian Wolf[3] and David Madlener[3]

[1] Purple Mountain Observatory & Key Laboratory for Radio Astronomy, Chinese Academy of Sciences, Nanjing 210008, China; *yliu@pmo.ac.cn*
[2] Graduate University of Chinese Academy of Sciences, Beijing 100049, China
[3] Institut für Theoretische Physik und Astrophysik, Universität zu Kiel, Leibnizstr. 15, 24118 Kiel, Germany

Received 2013 February 4; accepted 2013 March 22

Abstract We present modeling work on three young stellar objects that are promising targets for future high-resolution observations to investigate circumstellar disk evolution. The currently available data comprise the spectral energy distribution from optical to millimeter wavelengths which allow constraining the structure of the circumstellar disk using self-consistent radiative transfer models. The results suggest that the assumption of well-mixed dust and gas leads to overestimation of flux in the far-infrared. Observational and theoretical arguments suggest that an overall decrease in far-infrared excess can be explained by dust settling towards the midplane. A new disk model is hence employed to take the effect of dust sedimentation into account. The extended model satisfactorily reproduces all existing observations. The three targets studied here therefore deserve follow-up observations to reveal the evolutionary state of their protoplanetary disks.

Key words: circumstellar matter — planetary systems: protoplanetary disks — radiative transfer

1 INTRODUCTION

Circumstellar disks around pre-main sequence stars have been intensively studied in recent years because they are generally believed to be the birthplace of planets. Within these protoplanetary disks, dust grows from submicron-sized grains, as typically found in the interstellar medium (ISM), until a planetary size is reached through a not yet completely understood mechanism (e.g., Pollack et al. 1996; Lissauer & Stevenson 2007). During this coagulation process, large dust grains decouple from the turbulent gas flow and settle towards the disk midplane driven mainly by the gravity of the central star (e.g., Papaloizou & Terquem 2006; Carballido et al. 2006). Grain growth and settling of dust are therefore considered to be an initial step in the process of planet formation (Dominik et al. 2007). Moreover, these processes may be the driving cause for the transition of disk structure during the early phase of planet formation, such as flattening of the disk (Dullemond & Dominik

* Supported by the National Natural Science Foundation of China.

Table 1 Target Properties

Object Name	SpT	$T_{\rm eff}$ [K]	$L_\star$ [$L_\odot$]	$M_\star$ [$M_\odot$]	Age [Myr]	$A_{\rm v}$ [mag]	Cloud	Distance [pc]
LZK 21	M0	3850	1.46	0.55	0.75	6.00	Perseus	250
Cl*IC 348 LRL 265	M3	3415	0.42	0.32	1.47	17.0	Perseus	250
SSTc2d J182947+003223	M0	3850	0.28	0.58	5.81	7.00	Serpens	260

Notes: The data, except for stellar mass and age, are taken from Merín et al. (2010). The stellar mass and age are derived by interpolating the pre-main-sequence evolutionary tracks given in Siess et al. (2000).

2004a,b). Investigation of this crucial phenomenon can therefore provide important insights into how the formation of planets relates to the overall evolution of circumstellar disks.

The spectral energy distribution (SED) contains abundant information about disk geometry and dust properties. The shallow spectral index at (sub)millimeter wavelengths widely present in the observed SEDs of young stellar objects (YSOs) implies that dust grain size has already increased by orders of magnitude as compared to primordial ISM dust (e.g., Ricci et al. 2010a,b). Infrared (IR) spectroscopy provides hints of dust growth in circumstellar disks. Dust grains with average sizes above a few μm show only a weak spectral structure (e.g., the $10\,\mu$m silicate feature) and do not contribute significantly to the IR emission (e.g., van Boekel et al. 2005; Schegerer et al. 2006; Dominik et al. 2007). Dust settling is directly linked to the vertical structure of the disk. Observations show that most T Tauri stars and a subset of Herbig Ae/Be stars, such as the group II sources in Meeus et al. (2001), exhibit less mid- and far-IR excess than expected for a disk in which dust and gas are well mixed and coupled (e.g., Furlan et al. 2005, 2006; Juhász et al. 2010). Chiang et al. (2001) explained this characteristic by mimicking dust settling through an artificial reduction of the disk scale height. Self-consistent simulations of dust sedimentation produce similar SEDs with depressed emission at mid- to far-IR wavelengths, convincingly supporting the notion of dust settling in circumstellar disks (e.g., Dullemond & Dominik 2004a,b; D'Alessio et al. 2006).

Hence, analysis and modeling of the SED can be used to identify promising objects for the study of disk evolution with further high-resolution observations. Following this approach, Liu et al. (2012) found that an inclusion of grain growth and settling into the disk model significantly improves the interpretation of the observed SED of DoAr 33. In this paper, we continue in this direction and focus on SED fitting for three T Tauri stars located in nearby star formation regions. Merín et al. (2010) investigated 35 YSOs selected from the *Spitzer* "From Molecular Cores to Planet-Forming Disks" (c2d) catalog (Evans et al. 2009) with the goal of identifying and characterizing disks with inner holes, i.e. cold disks in their nomenclature. They derived the parameters of the inner hole from SED modeling using a well-mixed model with homogeneous grain size distribution. Note that their best fit significantly overpredicts the observed $70\,\mu$m flux for the targets LZK 21, Cl*IC 348 LRL 265 and SSTc2d J182947 + 003223, see figure 9 in Merín et al. (2010). The properties of these objects, for instance the stellar temperature and luminosity, are listed in Table 1. The photometric measurements available at different wavelengths are compiled and shown in Figure 1. The observed SEDs display a drop or flat spectrum at $\sim$70 μm, an unusual feature for typical YSOs (Lada 1999) and comparable to the case of DoAr 33. As dust settling is efficient in steepening the SED at mid- to far-IR wavelengths (Dullemond & Dominik 2004b), this feature makes these objects as promising as DoAr 33 for finding signs of disk evolution. Additionally, the millimeter measurements with the IRAM radio telescope allow us to constrain the dust mass in their circumstellar disks, and also reduce SED model degeneracy.

2 RADIATIVE TRANSFER MODELING

We use the Monte Carlo radiative transfer code `MC3D` developed by Wolf (2003) to simulate continuum observations. Our program includes multiple and anisotropic scattering and self-consistently

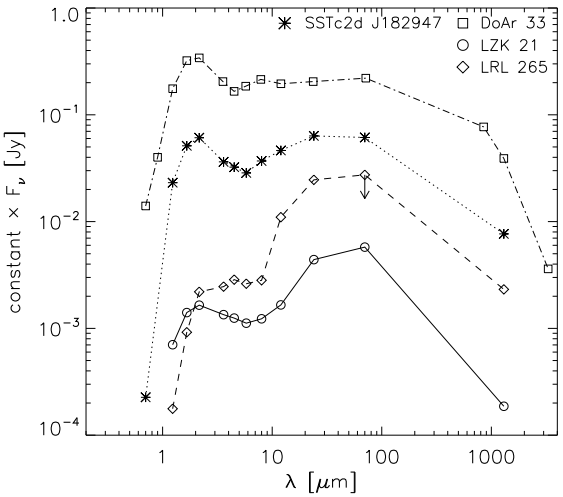

Fig. 1 Photometric measurements of the three selected sources. The data point at 12 μm is from the WISE All-Sky Data Release, and the rest of the photometry is taken from Merín et al. (2010). The observed SED of DoAr 33 is shown here for comparison (Liu et al. 2012).

calculates the temperature distribution of the dust using the scheme by Bjorkman & Wood (2001). The disk configuration is identical to the model adopted in Liu et al. (2012), which is briefly summarized here.

We first employ a so-called well-mixed prescription that parameterizes the standard model for an accreting disk introduced by Shakura & Sunyaev (1973). The dust distribution follows a Gaussian vertical profile

$$\rho_{\rm dust}(R,z) = \rho_0 \left(\frac{R_\star}{R}\right)^\alpha \exp\left[-\frac{1}{2}\left(\frac{z}{h(R)}\right)^2\right], \quad (1)$$

where R is the radial distance from the star in the equatorial plane, $R_\star$ the stellar radius, and ρ_0 a proportionality factor determined by normalizing the total dust mass. The disk extends from an inner radius $R_{\rm in}$ to an outer radius $R_{\rm out} = 200\,{\rm AU}$, which is consistent with the typical sizes found for T Tauri disks (Andrews & Williams 2007). Disk flaring is allowed by adjusting the scale height according to the power law

$$h(R) = h_{100}\left(\frac{R}{100\,{\rm AU}}\right)^\beta, \quad (2)$$

with the scale height h_{100} at a distance of 100 AU and the flaring exponent β. The dust properties are assumed to be homogeneous throughout the system. The grain size distribution follows a power law $n(a) \propto a^{-3.5}$ with diameters ranging from $a_{\rm min} = 5\,{\rm nm}$ to $a_{\rm max} = 1\,{\rm mm}$. The dust grain ensemble consists of smoothed astrophysical silicate and graphite with relative abundances of 62.5% silicate and 37.5% graphite (Weingartner & Draine 2001).

Theories of circumstellar disk evolution assume that dust grains coagulate and grow within the disk, and subsequently settle towards the midplane. To take this effect into account, we modify the standard flared disk model described above following the idea of D'Alessio et al. (2006). The upgraded model consists of two layers that are populated with different grain size distributions. The upper layer represents a population of small grains, whereas the deeper layer close to the disk midplane contains large dust grains. The scale height of the small grain population $h_{\rm small}$ is identical

to the canonical parameter from Equation (2), while the scale height $h_{\rm large}$ for the settled layer is given by the relation

$$h_{\rm large} = h_{\rm small}/H_{\rm ratio}. \quad (3)$$

As settling transfers mass from the upper layers towards the midplane, a parameter ϵ is hence introduced to quantify the depletion of small dust grains relative to the standard dust-to-gas mass ratio $\zeta_{\rm ISM} = 0.01$ found in the ISM

$$\epsilon = \frac{\zeta_{\rm small}}{\zeta_{\rm ISM}}, \quad (4)$$

where $\zeta_{\rm small}$ is the dust-to-gas mass ratio of the small grain population. The direct consequence of varying ϵ is to adjust the opacity to the stellar radiation and thus the height of the irradiation surface (D'Alessio et al. 2006). We adopt the same chemical composition and size distribution as discussed for both grain populations, but assume different maximum grain radii. The deeper layer features a larger value of $a_{\rm max} = 1\,{\rm mm}$, whereas we take $a_{\rm max} = 0.25\,\mu{\rm m}$ for the upper layer to mimic unprocessed ISM dust.

The disk is presumed to be passively heated by the stellar irradiation. We take the stellar parameters derived by Merín et al. (2010) as fixed inputs for the SED modeling of each source, and the NextGen spectra with $\log\,{\rm g} = 3.5$ and solar metallicity as the incident stellar spectrum (Hauschildt et al. 1999).

3 RESULTS AND DISCUSSION

Based on the two disk models laid out in the previous section, i.e. the well-mixed and settled scenario, we are left with a parameter space having six or eight adjustable parameters to reproduce the observed SEDs. Simulated annealing (SA), a versatile optimization technique based on the Metropolis-Hastings algorithm, is used to search for the best fit (Kirkpatrick et al. 1983). Details about the implementation of SA for the SED-fitting task can be found in the appendix of Liu et al. (2012). We propagated 12 different Markov chains for both the well-mixed and settled disk model. All Markov chains were terminated using the same criterion for consistency. The difference $\Delta\chi^2$ between two adjacent accepted steps can be considered as the measure of variation in fitting quality. A Markov chain is terminated if the box average $\langle\Delta\chi^2\rangle$ stays below a user-defined threshold $\Delta\chi^2_{\rm abort}$ for 100 consecutive steps. We use $\Delta\chi^2_{\rm abort} = 100$ and average with a box of 10 samples. With this abortion rule, there are typically $\sim$1000 steps performed in a chain. The best-fit parameter set is identified as the one with the lowest χ^2 found among all the chains.

We started the parameter study with the simpler well-mixed model. The predicted fluxes of the best-fit models found by SA are over-plotted with photometric measurements in Figure 2; see the blue dash-dotted lines. The corresponding parameter sets are listed in Table 2, where models w1, w2 and w3 represent the best fits for LZK 21, LRL 265 and SSTc2d J182947 respectively. In the fitting procedure, we used the extinction law of Cardelli et al. (1989) and $R_{\rm v} = 3.1$ to correct the model fluxes. The extinction and the distance to our targets are fixed and given in Table 1. The well-mixed model overpredicts the far-IR flux for all three objects, particularly at MIPS 70 μm. Similar results can be seen in figure 9 of Merín et al. (2010). Using our own radiative transfer code and fitting tool, we confirm that the standard model is not sufficient to explain the observed far-IR photometry. The drop in flux at $\sim$70 μm suggests dust settling caused by slow sedimentation of dust grains toward the disk midplane driven mainly by the gravitational attraction of the central star. This process can be accelerated by grain growth because larger grains have shorter settling timescales in circumstellar disks (Dominik et al. 2007). Moreover, dust sedimentation is relatively effective in quiescent disks or disks with weak turbulence (Nomura & Nakagawa 2006). The overall effect of dust settling toward the midplane is to decrease the scale height of the disk's photosphere (Dullemond & Dominik 2004b; D'Alessio et al. 2006). The disk is hence flattened and heated less efficiently, leading to less excess emission at mid- and far-IR wavelengths.

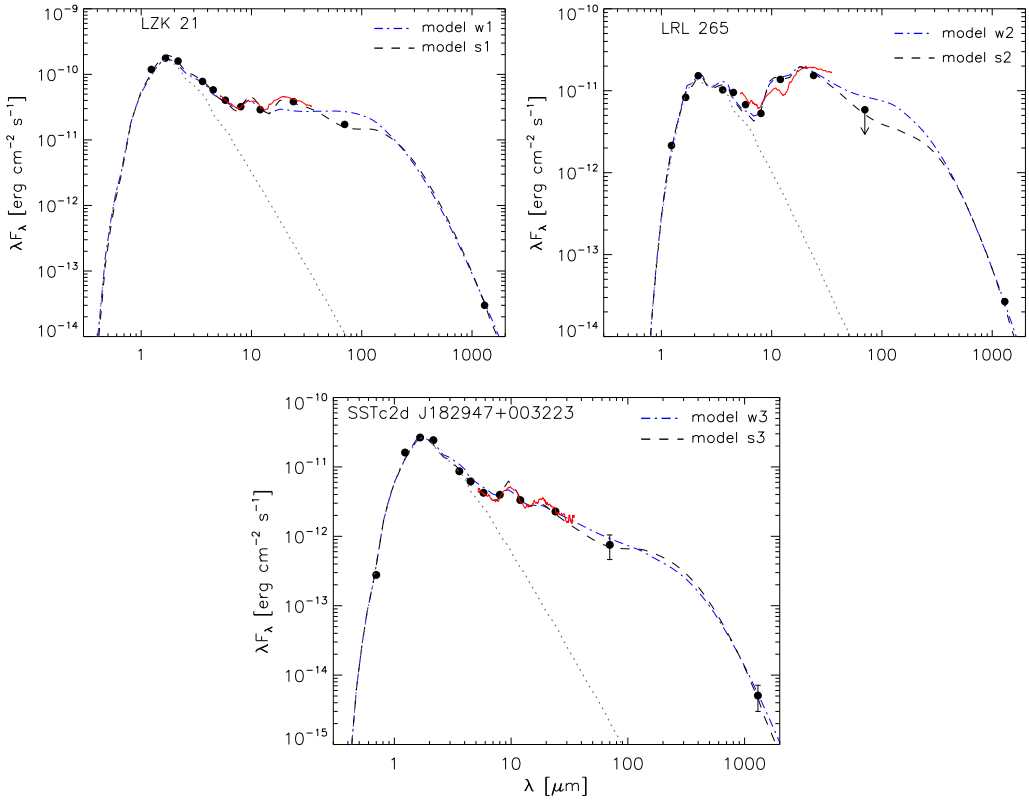

Fig. 2 The best-fit models found by the SA algorithm using the well-mixed (w1, w2, w3; *dash-dotted lines*) and settled disk model (s1, s2, s3; *dashed lines*) described in Sect. 2. The black dots depict the photometric measurements and the red solid lines represent the spectrum from Spitzer/IRS (Merín et al. 2010). Error bars for the photometry are shown if they are larger than the symbol. The gray dotted lines mark the contribution of the central star to the total flux of the system.

Table 2 The Parameter Sets of the SED Models Shown in Fig. 2

Parameter	Model					
	w1	s1	w2	s2	w3	s3
$R_{\rm in}$ [AU]	0.11	0.09	1.65	1.64	0.07	0.18
$M_{\rm dust}$ [$10^{-5}\,M_{\odot}$]	6.7	7.6	7.9	9.3	3.8	2.7
α	2.21	2.72	2.18	2.15	2.75	1.91
β	1.19	1.30	1.18	1.16	1.11	1.17
h_{100} [AU]	11.64	12.15	8.50	9.51	7.19	16.95
$H_{\rm ratio}$	1.00	2.89	1.00	1.85	1.00	9.59
ϵ	1.00	0.63	1.00	0.52	1.00	0.01
i [°]	28	32	45	35	54	30
χ^2	3133	502	1862	1306	116	77

If the sedimentation height $H_{\rm ratio}$ and the depletion parameter ϵ tend toward 1, and the maximum grain size $a_{\rm max}$ for both the small and large grain populations are identical, then the settled disk model turns into the well-mixed scenario.

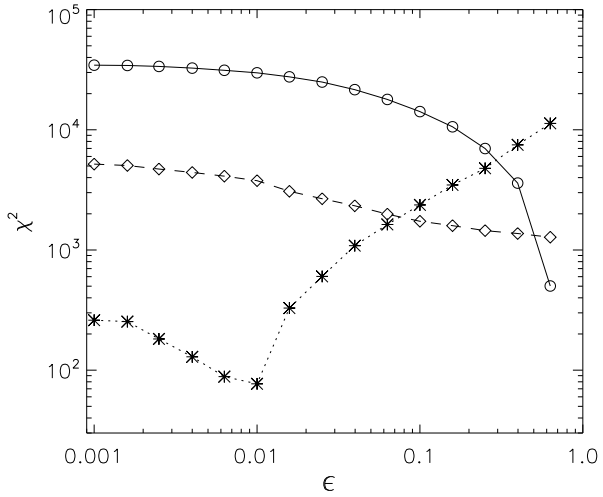

Fig. 3 χ^2 evolution with the depletion parameter ϵ. The symbols are the same as used in Fig. 1. Note that all of the other parameters are fixed to the best fit values, see Table 2. This is because varying different parameters simultaneously cannot directly show the SED dependence on a single variable due to the model degeneracy.

The black dashed lines shown in Figure 2 indicate the best matches using the settled disk model. The corresponding parameter sets are given in Table 2, where we designate the models with a lowercase "s." The results demonstrate that settling can satisfactorily explain the observed data for all three targets. SED analysis places strong constraints on the disk inner radius and dust mass because both scenarios return similar results for these two parameters. Moreover, we found that a large value for the inner radius (i.e. $R_{\rm in}{\sim}1.6\,{\rm AU}$) is necessary to reproduce the prominent dip feature in the IR SED of LRL 265, which is consistent with the characteristics of so-called transition disks (e.g., Cieza et al. 2010, 2012). However, our modeling work suggests little dissipation of dust in the inner region of the disks surrounding LZK 21 and SSTc2d J182947 because the best-fit inner radius is close to the dust sublimation radius for both objects. Small dust grains are effective absorbers at short wavelengths, especially in the optical and near-IR domain where the central star dominates the radiation field. As the parameter ϵ quantitatively describes the degree of depletion of small grains in the disk's upper layer, it plays an important role in affecting the IR emission of the system. In order to explore the dependence of the SED on this variable, we investigated how the χ^2 changes with different values of ϵ. The result is shown in Figure 3. It is clear to see that settling of small dust has an obvious impact on the results for LZK 21 and SSTc2d J182947. However, this effect is not pronounced for LRL 265. This is because a large inner hole ($R_{\rm in}{\sim}1.6\,{\rm AU}$) is present in the circumstellar disk. In this case, sedimentation occurs at a large radial distance and hence does not significantly change the temperature structure (especially in the hot part) of the disk. The best-fit depletion parameter of all three targets, $\epsilon < 1$, is consistent with the fact that a portion of the small grain population has undergone coagulation and settled towards deeper layers of the disk. This depletion of upper layers leads in turn to a reduction in IR excess and an overall steepening of the SED in the mid- and far-IR regimes.

There may be an alternative explanation for the flux decrease at $\sim$70 μm that does not involve two different grain size populations. Dullemond & Dominik (2004a) introduced a self-shadowed disk model to explain the observed SEDs of the group II Herbig Ae/Be sources in Meeus et al.

(2001) that exhibit very weak far-IR excess. The disk is assumed to be truncated on the inside at the dust sublimation radius. Because of its direct exposure to the stellar flux, the inner edge of the disk is much hotter than the rest of the disk and forms a puffed-up inner rim that casts a shadow over the disk behind it. The material outside the inner rim will lie in the shadow and not be directly illuminated, leading in turn to a reduction in IR flux. As discussed by Dullemond et al. (2001), this puffed-up inner rim will also cause a conspicuous near-IR excess that naturally explains the observed near-IR bump at $\sim 2\,\mu\mathrm{m}$ that is commonly present in the SEDs of Herbig Ae systems (Natta et al. 2001). However, this explanation is inconsistent with the fact that all sources in our study show negligible near-IR excess, see Figure 2. Self-shadowing can therefore be excluded from our target disks.

Model degeneracies are an omnipresent accessory phenomenon of modeling a spatially integrated observable like the SED. However, our detailed modeling effort indicates that an inclusion of dust growth and settling into the disk model highly improves the interpretation of the existing data. Although some constraints on disk structure and dust properties can be deduced by fitting SED data, the results are not definitive. Follow-up observations are necessary to reduce the inherent model degeneracy and identify possible model refinements. Photometric measurements in the (sub)millimeter regime will enable the estimation of the spectral slope at this wavelength domain, which is a good diagnostic tool to estimate the presence of large grains. Herschel far-IR photometry can bridge the gap between the mid-IR and millimeter wavelengths, and help to improve the constraints on the scale heights and flaring exponent β, especially the depletion ϵ of the disk. High-resolution images taken at different wavelengths, e.g. with the Atacama Large Millimeter Array (ALMA), will break the SED model degeneracies and place additional constraints on the grain size and spatial dependency of the dust properties in the circumstellar disk.

4 SUMMARY

We conducted detailed SED modeling for three T Tauri stars located in nearby star formation regions and found that a standard well-mixed model fails to explain the available data. In particular, the predicted far-IR fluxes at $\sim 70\,\mu\mathrm{m}$ significantly exceed the observations. This discrepancy can be considered as a key sign for dust coagulation and settling towards the midplane of the protoplanetary disks, as these processes are expected to induce this effect on the SED. For this reason, we modified the standard model by dividing the flared disk into two layers differing in terms of grain size distribution and vertical scale height. We assume the dust in the upper layer to have the properties of the well-known MRN distribution found in the ISM (Mathis et al. 1977), and set the maximum grain radius to $1\,\mathrm{mm}$ in the settled grain population to account for dust evolution by coagulation. Simulated annealing was adapted to the radiative transfer code `MC3D`, and used to search for the best-fit parameter sets. Our results show that the predictions of the upgraded model satisfactorily match the observations in all wavelength regimes. We conclude that the three objects in our study are promising candidates for the investigation of dust growth and sedimentation. Additionally, we also briefly discussed other scenarios for the disk model, such as disks with self-shadowing geometry as an interpretation of the observed disk properties. Follow-up observations, especially high-resolution imaging at multiple wavelengths, are needed to unveil the structure and evolution of the disks surrounding these fascinating objects.

Acknowledgements H.W. acknowledges support by the National Natural Science Foundation of China (Grant Nos. 10733030, 10921063 and 11173060). We acknowledge the anonymous referee for comments and suggestions that helped to improve this paper. This publication makes use of data products from the Wide-field Infrared Survey Explorer, which is a joint project of the University of California, Los Angeles, and the Jet Propulsion Laboratory/California Institute of Technology, funded by the National Aeronautics and Space Administration.

References

Andrews, S. M., & Williams, J. P. 2007, ApJ, 659, 705
Bjorkman, J. E., & Wood, K. 2001, ApJ, 554, 615
Carballido, A., Fromang, S., & Papaloizou, J. 2006, MNRAS, 373, 1633
Cardelli, J. A., Clayton, G. C., & Mathis, J. S. 1989, ApJ, 345, 245
Chiang, E. I., Joung, M. K., Creech-Eakman, M. J., et al. 2001, ApJ, 547, 1077
Cieza, L. A., Schreiber, M. R., Romero, G. A., et al. 2010, ApJ, 712, 925
Cieza, L. A., Schreiber, M. R., Romero, G. A., et al. 2012, ApJ, 750, 157
D'Alessio, P., Calvet, N., Hartmann, L., Franco-Hernández, R., & Servín, H. 2006, ApJ, 638, 314
Dominik, C., Blum, J., Cuzzi, J. N., & Wurm, G. 2007, Protostars and Planets V, 783
Dullemond, C. P., Dominik, C., & Natta, A. 2001, ApJ, 560, 957
Dullemond, C. P., & Dominik, C. 2004a, A&A, 417, 159
Dullemond, C. P., & Dominik, C. 2004b, A&A, 421, 1075
Evans, N. J., II, Dunham, M. M., Jørgensen, J. K., et al. 2009, ApJS, 181, 321
Furlan, E., Calvet, N., D'Alessio, P., et al. 2005, ApJ, 628, L65
Furlan, E., Hartmann, L., Calvet, N., et al. 2006, ApJS, 165, 568
Hauschildt, P. H., Allard, F., Ferguson, J., Baron, E., & Alexander, D. R. 1999, ApJ, 525, 871
Juhász, A., Bouwman, J., Henning, T., et al. 2010, ApJ, 721, 431
Kirkpatrick, S., Gelatt, C. D., & Vecchi, M. P. 1983, Science, 220, 671
Lada, C. J. 1999, in NATO ASIC Proc. 540: The Origin of Stars and Planetary Systems, eds. C. J. Lada, & N. D. Kylafis, 143
Lissauer, J. J., & Stevenson, D. J. 2007, Protostars and Planets V, 591
Liu, Y., Madlener, D., Wolf, S., Wang, H., & Ruge, J. P. 2012, A&A, 546, A7
Mathis, J. S., Rumpl, W., & Nordsieck, K. H. 1977, ApJ, 217, 425
Meeus, G., Waters, L. B. F. M., Bouwman, J., et al. 2001, A&A, 365, 476
Merín, B., Brown, J. M., Oliveira, I., et al. 2010, ApJ, 718, 1200
Natta, A., Prusti, T., Neri, R., et al. 2001, A&A, 371, 186
Nomura, H., & Nakagawa, Y. 2006, ApJ, 640, 1099
Papaloizou, J. C. B., & Terquem, C. 2006, Reports on Progress in Physics, 69, 119
Pollack, J. B., Hubickyj, O., Bodenheimer, P., et al. 1996, Icarus, 124, 62
Ricci, L., Testi, L., Natta, A., & Brooks, K. J. 2010a, A&A, 521, A66
Ricci, L., Testi, L., Natta, A., et al. 2010b, A&A, 512, A15
Schegerer, A., Wolf, S., Voshchinnikov, N. V., Przygodda, F., & Kessler-Silacci, J. E. 2006, A&A, 456, 535
Shakura, N. I., & Sunyaev, R. A. 1973, A&A, 24, 337
Siess, L., Dufour, E., & Forestini, M. 2000, A&A, 358, 593
van Boekel, R., Min, M., Waters, L. B. F. M., et al. 2005, A&A, 437, 189
Weingartner, J. C., & Draine, B. T. 2001, ApJ, 548, 296
Wolf, S. 2003, Computer Physics Communications, 150, 99